Resonance and damping characteristics of cryogenic fusion targets

Harvest Zhang

Brighton High School
Rochester, NY

Advisor: Mr. L. D. Lund

Laboratory for Laser Energetics
University of Rochester
Rochester, NY
November 2009

Abstract

Targets for direct drive inertial confinement fusion experiments on the OMEGA Laser at the University of Rochester were tested on a shaker apparatus to determine target motion behavior under vibrational excitation. Frequency response functions were used to determine that each target has two distinct dominant resonance frequencies, one for each principal axis, both around the 130-150 Hz range. Damping was estimated by the half-power bandwidth and exponential decay methods to be around 1% of critical damping. Both methods gave almost identical values for the damping within the experimental uncertainties. Target displacement given an applied acceleration was measured to be within the 300-400 μm/gn range. A program was written to visualize three-dimensional target motion at high frame rates to investigate cross-coupling, the excitation of vibrations in the target along an axis transverse to the direction of applied acceleration. The visualization confirms the existence of distinct target resonance axes. The data obtained and methods developed to analyze target behavior will eventually help to design improved target support structures, which will reduce target vibration induced by equipment in the target chamber during a laser shot, resulting in better alignment, higher radiation uniformity and thus higher fusion reaction efficiency.

1 Introduction

Nuclear fusion promises to provide a sustainable and environmentally safe form of energy for the future. Several large facilities, including the National Ignition Facility in Livermore, CA and the Laser Megajoule in France, are experimenting with inertial confinement fusion, where a spherical capsule containing hydrogen fuel is heated and compressed by a large number of laser beams to yield alpha particles, neutrons, and a large amount of energy [1]. At the

Laboratory for Laser Energetics at the University of Rochester, fusion experiments are carried out on the 60-beam OMEGA laser [2].

The laser radiation must be distributed as uniformly as possible over the surface of the capsule to ablate the surface evenly and create a uniform implosion. This requires a smooth capsule surface and proper alignment of the capsule in the center of the target chamber [3]. It is therefore crucial for the capsule to be stationary in order to achieve uniform irradiation.

There are various sources of excitation of target motion in the target chamber. The cryogenic pumps create a steady state vibration, and the thermal shroud that covers the target transiently excites the target when it is pulled upwards to clear the target for the shot [4], [5]. Therefore, it is important to know how a target behaves over a large range of frequencies and how well the target damps out after the excitation.

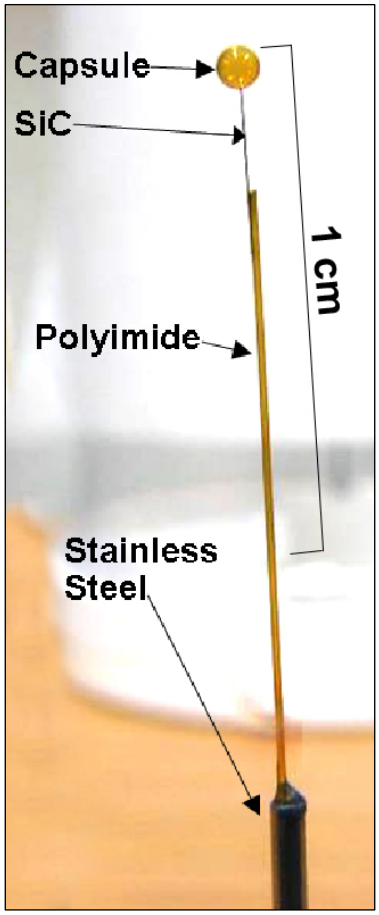

Fig. 1 Photo of a mass equivalent fusion target
The capsule is mounted on a very long stalk that is subject to vibration. Note the asymmetry at the joints between materials, which results in two dominant resonance frequencies in two principal axes at right angles to each other.

A typical target used in OMEGA laser fusion experiments is shown in Fig. 1. The capsule, with a diameter of just under 1 mm, is glued on top of an approximately 2 mm long SiC fiber with a diameter of 17 µm. This stalk is then glued to the outside of a polyimide tube a little over a centimeter long, and the polyimide tube is then fixed inside a stainless steel tube which is attached to the base of the target assembly (not shown in Fig. 1). The entire target, including the base, stalk, and capsule, has a mass of just under 0.2 g, with an overall length of just under 34 mm.

The capsules needed for fusion are thin plastic shells only 5 μm thick, on the inside of which there is a 100 μm layer of cryogenic deuterium and tritium ice at 20 K. As the mass of the capsule affects target behavior under vibration, the capsules tested at room temperature have thicker plastic walls but no deuterium-tritium, so that the mass of a test capsule is equivalent to the mass of a deuterium-tritium filled capsule.

In these experiments, targets were tested in a shaker apparatus, which applied vibrational excitations to the target at various frequencies. The dominant resonance frequencies, transmissibility (capsule displacement divided by applied acceleration), and amount of damping were measured by two different methods. A program was also written to aid visualization of the path of target motion under excitation. The data suggests that these targets resonate at two distinct frequencies in the 130 Hz to 150 Hz range in the directions of the principal axes. Additionally, increased target stiffness was found to correlate with increased resonance frequencies, decreased transmissibility, and decreased damping. These findings are helpful to the search for better materials and designs for target support structures, which will eventually be optimized to minimize target vibration.

2 Experimental

2.1 The shaker apparatus

A shaker apparatus is used to excite the target. The base of the target's stalk magnetically mounts into a collet on the shaker stage, which is connected to a shaker driver that provides acceleration in the X direction. Two quadrant-cell photoreceivers [6] detect the position of the capsule, one in each of the shaker's X and Y directions, and an accelerometer attached to the

stage measures input acceleration in the X direction. The position data collected is then transferred by means of an analog-to-digital converter [7] to a computer program.

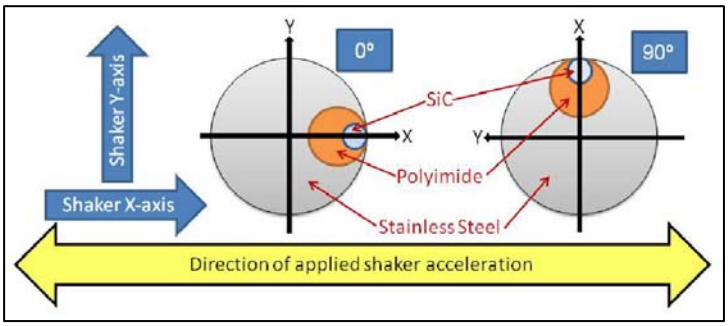

Fig. 2 Overhead diagram of shaker and target axes
The target's X and Y axes rotate with the target, while the shaker's axes remain constant. The shaker always applies acceleration in its X-axis direction.

Targets were tested in two orientations to account for their design asymmetry. As shown in Fig. 2, the target's X-axis is defined as a line drawn in the X-Y plane which intersects both the center of the stainless steel tube and the two points of tangency where the different materials join together. In the 0º position, the target's X and Y axes line up with the shaker's X and Y axes, and the target's X-axis is longitudinally excited. In the 90º orientation the target is rotated about the Z-axis, and the target Y-axis is longitudinally excited.

Using this setup, target behavior and damping are measured by two different methods as described in the next two sections.

2.2 Frequency response functions and half-power bandwidth damping

The target's motion at the capsule can be approximated by treating it as a driven, damped single degree of freedom oscillator [8]. The capsule is thus treated as a particle subject to an oscillatory force at frequency ω provided by the shaker, a restoring force proportional to its displacement, and a damping force proportional to velocity. The particle's position is given by the real part of the complex position $x(t)$, which obeys the equation of motion

$$\frac{d^2x}{dt^2} + \gamma\frac{dx}{dt} + \omega_0^2 x = a_0 e^{i\omega t} \qquad (1)$$

where γ is the damping constant, ω_0 is the resonance frequency, and a_0 is the amplitude of the applied force divided by the particle's mass. Setting $x=x_0e^{i\omega t}$ where x_0 is the amplitude of oscillation, we can derive the complex transmissibility T, which is defined as x_0/a_0:

$$T = \frac{x_0}{a_0} = \frac{1}{\omega_0^2 + i\omega\gamma - \omega^2}. \qquad (2)$$

The modulus of T, when plotted against frequency as in Fig. 3(a), is known as the frequency response function (FRF). Its units are distance divided by acceleration in units of gravity. In order to obtain an FRF, the shaker is used to output sine waves in chirps, each chirp sweeping through a range of frequencies, and the displacements of the capsule in the X and Y directions and the acceleration applied to the shaker stage during the chirp are measured. A fast Fourier transform is used to convert this time-domain data into the frequency-domain FRF [6]. The domain was set at 0 Hz to 500 Hz, giving a frequency resolution of 0.3125 Hz, as the analog-to-digital converter is only capable of 1600 lines of resolution. Thirty chirps are performed, and the resulting FRFs are averaged. The phase of T was plotted in Fig. 3(b) as the phase function.

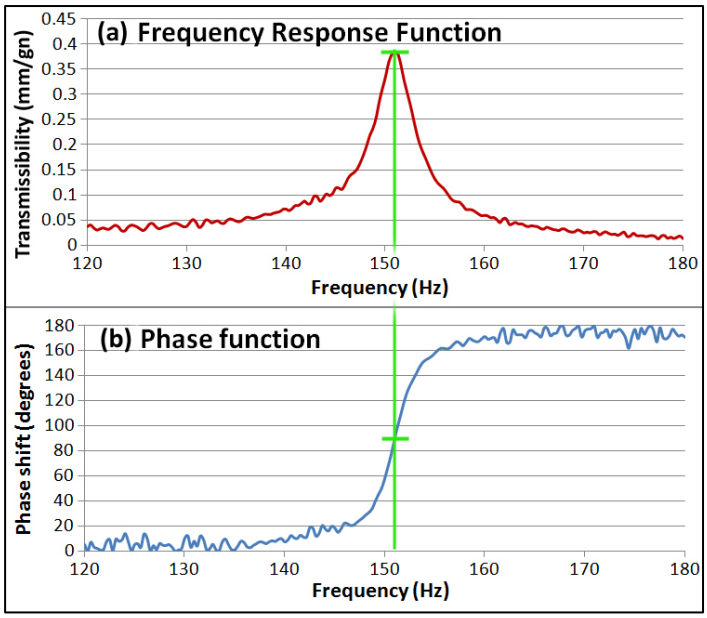

Fig. 3 A typical target frequency response function (a) and phase function (b).
The green cursor shows the resonance frequency at which the transmissibility has its peak, the same frequency at which the phase function, the phase of the complex transmissibility without the negative sign, crosses 90°.

Equation (2) indicates that away from resonance, the $i\omega\gamma$ term is negligible due to the γ term being very small. Thus, x_0/a_0 will be positive for applied frequencies lower than ω_0,

meaning that the displacement is in phase with the acceleration, resulting in a phase shift of 0º left of resonance. Similarly, x_0/a_0 will be negative for applied frequencies higher than ω_0, meaning that the displacement is out of phase with the acceleration, resulting in the 180º phase shift right of resonance in Fig. 3. At resonance ($\omega=\omega_0$), the displacement and acceleration are 90º out of phase. Resonance frequencies from FRFs were confirmed to line up with the frequencies at which the phase function is at 90º.

Coherence data, which measures the degree to which the input acceleration oscillation and the target displacement oscillation have a constant relative phase, was also collected. High coherence at a certain frequency ensures that the transmissibility measured is truly the result of excitation at that frequency [7]. The coherence function was used only as a visual check to make sure that the coherence near the dominant resonance frequency was close to 100%.

Defining the half-power points as the frequencies in the FRF at which the square of the transmissibility is half the square of the resonance transmissibility, $|T|^2=(1/2)|T_0|^2$, it can be shown from Eq. (2) that the damping coefficient $\gamma = \Delta\omega$, the difference in frequency between the two half-power points. However, it is more useful to express the damping as the ratio γ/γ_c where γ_c is the critical damping (defined below), since this allows for comparisons between different targets. The general solution of the damping is found by removing the driving term from Eq. (1) and setting the complex displacement $x = x_0e^{i\omega t}$ (with complex ω), from which a quadratic equation can be solved for ω leading to two roots, giving

$$x = x_0\left(e^{-\frac{\gamma t}{2}}\right)\left(e^{\pm\frac{it}{2}\sqrt{-\gamma^2+4\omega_0^2}}\right) \qquad (3)$$

where the $e^{-\gamma t/2}$ term gives an exponential decay envelope and the other term gives an oscillation as long as $\gamma<2\omega_0$. Since critical damping is defined as the lowest possible value for damping that

will preclude all oscillation, the argument of the square root can be set equal to zero, leaving $\gamma_c = 2\omega_0$. Therefore, the damping ratio λ is given by

$$\lambda = \frac{\gamma}{\gamma_c} = \frac{\Delta\omega}{2\omega_0}. \qquad (4)$$

The *Damping Estimator* component of the graphical user interface (GUI) program *Target Motion Characterization* was written in Matlab to perform half-power bandwidth damping calculations. As seen on the right panel of Fig. 4, it identifies the resonance peak (large red circle), uses linear interpolation to approximate the half-power bandwidth points (smaller red circles), and then uses Eq. (4) to estimate the damping ratio as a percent of critical damping.

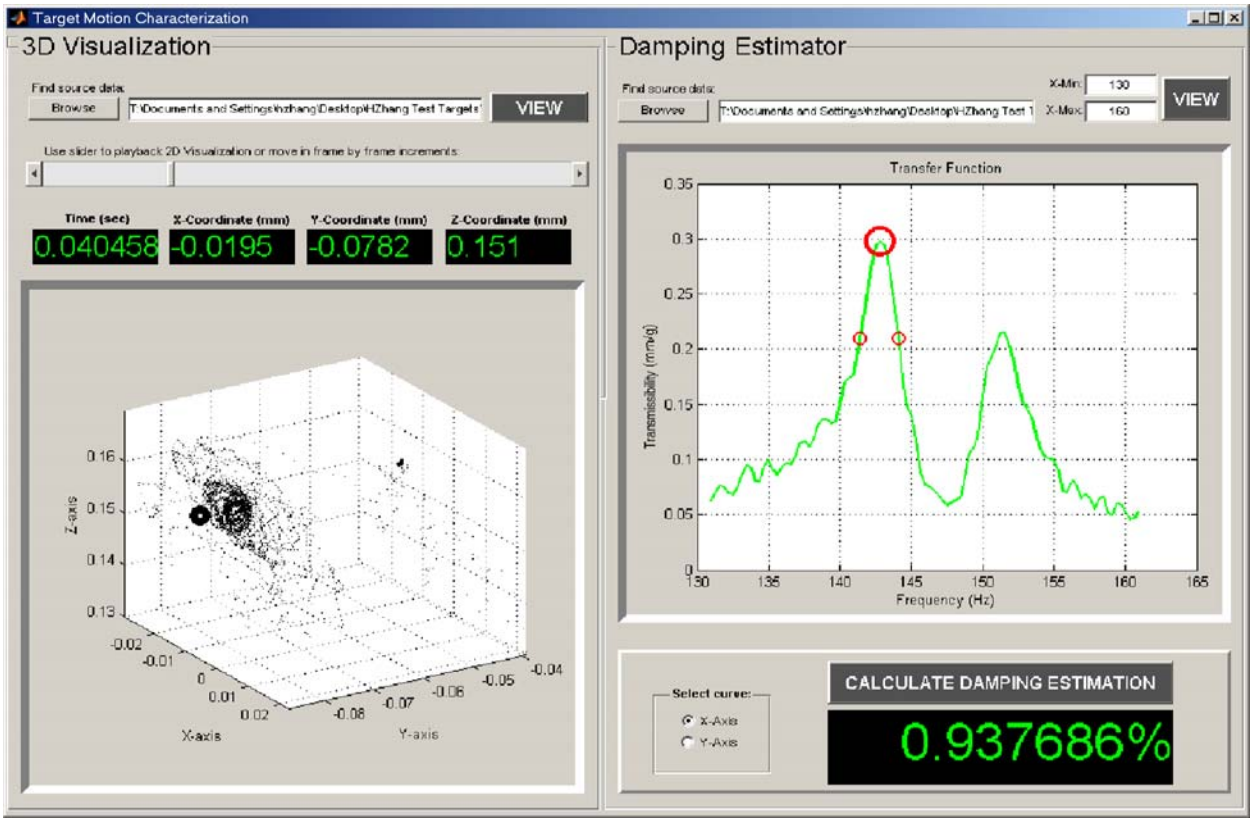

Fig. 4 The two components of the *Target Motion Characterization* GUI program
On the right is the *Damping Estimator* GUI. The large red circle indicates the resonance peak, and the smaller red circles indicate the half-power points. The damping ratio, shown at the bottom in green, has been calculated for this particular peak. On the left is the *3D Visualization* GUI, which displays a rotatable parametric plot of all the points in space the capsule occupies during an excitation. The thick black circle indicates the current position of the center of the capsule. The coordinates of the capsule and the time are displayed on the green readouts. The slider is used to play back the visualization, which is currently hardware limited to just under 100,000 frames per second.

2.3 Time-domain transient excitation and exponential decay damping

The exponential decay method of estimating damping uses transient excitations measured in the time domain. A sine wave excitation at the target's dominant resonance frequency (as found from the FRF) is applied, the goal being to excite only the dominant resonance mode. The duration of the excitation is set long enough so that the target reaches a maximum amplitude of vibration, at which point the excitation is turned off and the target undergoes a symmetrical, exponentially decaying series of oscillations at one frequency, as seen in Fig. 5.

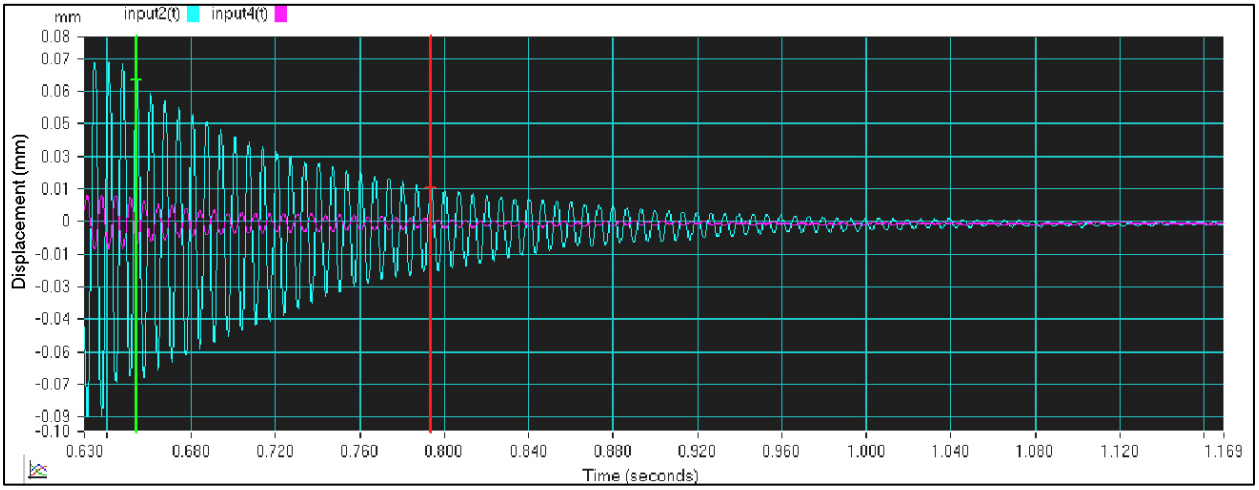

Fig. 5 A time-domain graph of target motion following a transient excitation at the resonance frequency
The X-axis displacement is shown in cyan and the Y-axis displacement (due to cross-coupling) in magenta. The green and red cursors indicate two peaks that are used to calculate the damping.

The damping coefficient γ can be measured directly from the exponential decay envelope term of Eq. (3), $A = A_0 e^{-\gamma t/2}$, where A is the amplitude of the oscillation. Equivalently, γ can be measured from any two peaks during the decay t_0 and t_n, with respective amplitudes A_0 and A_n, where the length of one period is given by $2\pi/\omega_0$. Recalling that $\gamma_c=2\omega_0$, it is easy to show that the damping ratio λ is given by

$$\lambda = \frac{\gamma}{\gamma_c} = \frac{1}{2\pi n} \ln \frac{A_0}{A_n}. \qquad (5)$$

A few issues remain; the shaker stage itself has a small but significant shift in the X-axis that is slow returning to 0 when the excitation is turned off, and slight errors in target alignment

set the stationary point a few microns above or below 0. Note that the peak displacement must be small (80 μm in Fig. 5) in order to prevent the capsule from falling off the stalk. To reduce the errors due to these effects, two positive peaks and the two following negative peaks are run through the calculations separately, and the values calculated are averaged so that the positive error in one measurement balances out the negative error in the other. Future calculations will implement an additional GUI in *Target Motion Characterization* which will minimize shaker-shift and positioning errors by averaging the positive and negative amplitudes of oscillation and then directly fitting an exponential decay curve to the resultant amplitudes.

2.4 Variability testing

Variability tests were carried out to determine the repeatability of the resonance frequency, transmissibility, and damping values calculated by both methods. Most of the variability involves the precision to which the target can be placed in the collet at exactly the same angle trial after trial; if the angle is even slightly off, the axes of the target and the shaker will not be directly aligned and thus the resonance frequency, transmissibility and damping ratio may change.

For the half-power bandwidth variability test, the target was first aligned in the 0º direction, tested once, removed from the collet, and then replaced in the collet as close to the same angle as could be visually determined. The measurements were taken again and this process was repeated seven times. The target was then rotated to the 90º orientation and the shaker was realigned so that the initial X and Y positions of the target were both at the origin. Seven more trials were taken in this orientation. The standard deviations were then calculated for the resonance frequency, the resonance transmissibility, and the damping ratio.

The exponential decay test was done in a similar way, except that due to the small amplitude of the target excitation, realignment was necessary for every trial in order to get the decay as centered about 0 mm as possible (see Fig. 5). Here, the goal was not just to determine precision across trials, but also to determine an optimum way of selecting peaks to use in the exponential decay calculation so as not to include the aforementioned errors regarding target alignment and shaker stage movement. Thus, seven trials were done in the 0º orientation and then repeated in the 90º orientation. The frequency of excitation was determined by the corresponding resonance frequency of each target axis, as found in the half-power variability test. For each single trial, transmissibility was calculated by dividing the peak steady state amplitude of the target at resonance by the peak acceleration delivered by the shaker driver. Six exponential decay damping values were taken per trial. The standard deviation was calculated for the transmissibility and the damping ratio.

2.5 3-dimensional high frame rate target visualization

As the second part of the program *Target Motion Characterization*, *3D Visualization* was written to better understand exactly where the target is during an excitation. It takes displacement data in all three axes over a period of time and then graphs the data parametrically, allowing a 3-dimensional playback of the target position frame by frame as well as an overall view of all the points where the target has been, as shown in the left side of Fig. 4. In this way, it is easy to gain a general idea of the target's range of motion, as darker areas represent areas where the target is found most frequently. The analog-to-digital converter currently limits the program to a maximum of 4096 frames at 96154 frames per second. The GUI allows for rotation of the graph and playback of the target at whichever viewing angle is of interest.

3 Results and Analysis

3.1 Frequency response functions and half-power bandwidth damping

Fig. 6 shows frequency response functions for target 2 in the tables below, oriented at 0º in Fig. 6(a) and 90º in Fig. 6(b). The red curves are FRFs of the target axis under longitudinal excitation. The blue curves are FRFs of the target axis under transverse excitation. The highest peaks in Fig. 6(a) and Fig. 6(b) are at different frequencies, confirming that the asymmetry of the targets results in different resonance behavior in different orientations.

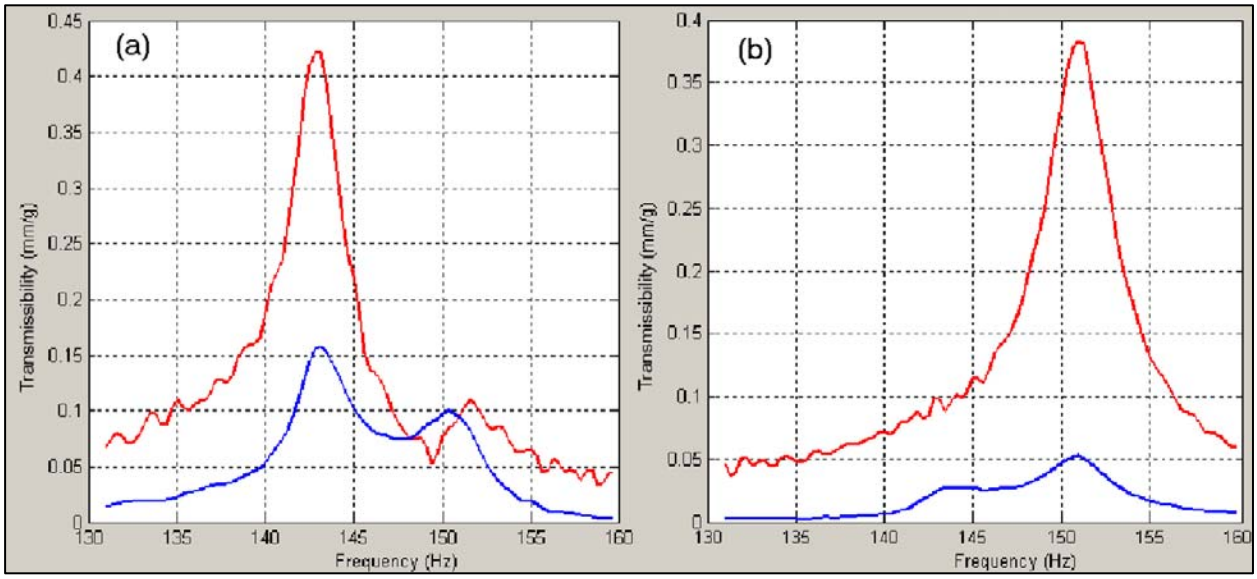

Fig. 6 Frequency response functions for (a) 0º and (b) 90º
The red curves show the target's motion under longitudinal excitation for the target's X-axis in (a) and the Y-axis in (b). The blue curves show the cross-coupled motion of the non-driven, transversely excited target axes.

A second peak is seen in the blue curve of Fig. 6(a), corresponding to the Y-axis resonance frequency. This occurs because the target was not placed in the collet at precisely 0º, causing a small amount of excitation at the Y-axis resonance frequency due to cross-coupling. Dual peak cases like this one are present in other targets for the same reason.

Usually, these peaks are less than 10 Hz apart, as is seen in Table 1, which gives the resonance frequencies for the three targets tested. Axes in all tables refer to the target's axes. An error of one standard deviation as determined by variability testing is reported for target 2 in this

and similar tables. The standard deviation is low due to the resolution being 0.3125 Hz; measurements either always return the same resonance frequency value, thus causing the 0.0 Hz standard deviation in the Y-axis of target 2, or alternate between two frequencies 0.3125 Hz apart, resulting in low standard deviations like the 0.15 Hz in the X-axis of target 2. Thus, the precision to which resonance frequency measurements can be made is limited by the resolution to about 0.3 Hz.

Table 1. X and Y resonance frequencies obtained from the frequency response function

FRF Method	X-axis	Y-axis
Target 1	148.8 Hz	145.6 Hz
Target 2	142.9 Hz ±0.15 Hz	150.9 Hz ±0.0 Hz
Target 3	134.1 Hz	135.9 Hz

Average resonance transmissibility values are given in Table 2. The precision of these measurements is questionable because the standard deviation is high, at 54 µm/gn for a 423 µm/gn measurement. These measurements seem to reflect a general trend of transmissibility close to 400 µm/gn, with no further precision determinable due to the high variability.

Table 2. X and Y resonance transmissibility obtained from the frequency response function

FRF method	X-axis	Y-axis
Target 1	410 µm/gn	389 µm/gn
Target 2	423 µm/gn ±54 µm/gn	378 µm/gn ±34 µm/gn
Target 3	449 µm/gn	454 µm/gn

Damping calculations from the half-power bandwidth method, however, showed greater precision. Table 3 shows the damping ratio present in these targets in the X and Y axes under longitudinal excitation. Considering that the standard deviation in the X axis is almost a tenth of a percent, this method estimates the damping ratio at 1% for all three targets.

Table 3. X and Y damping ratio obtained from the frequency response function

FRF method	X-axis	Y-axis
Target 1	1.1%	1.1%
Target 2	1.0% ±0.07%	1.1% ±0.01%
Target 3	1.2%	1.1%

3.2 Time-domain transient excitation and exponential decay damping

Table 4 shows resonance transmissibility data for targets 1 and 2. The input frequencies for each test are as measured for each target in Table 1.

Table 4. X and Y resonance transmissibility obtained from time-domain transient excitation

Time Domain	X-axis	Y-axis
Target 1	No data	404 µm/gn
Target 2	268 µm/gn ±12 µm/gn	249 µm/gn ±10 µm/gn

The transmissibility data from Table 4 is somewhat puzzling when compared with the corresponding data from the FRFs shown in Table 2. The Y-axis data for target 1 compares favorably, as the 404 µm/gn calculated from the transient excitation at resonance is within one standard deviation (34 µm/gn) of the 389 µm/gn obtained from the FRF. Target 2, however, shows a large discrepancy: 268 µm/gn and 249 µm/gn for transient excitation versus 423 µm/gn and 378 µm/gn from the FRF. A probable cause for this discrepancy is that the single applied excitation frequency could have been at a slightly different frequency from the target's actual resonance frequency. Future work would involve performing the same test with a series of different excitation frequencies near the resonance frequency. It is still worth noting that the standard deviations are much lower for transmissibility measured by this method, at a repeatability of about 10 µm/gn for a measurement around 250 µm/gn.

Damping ratios calculated by the exponential decay method are shown in Table 5. They generally agree with the values obtained from the half-power bandwidth method. The standard deviations are lower (0.01% and 0.02% in Table 5 for the X and Y axes, respectively, compared with 0.07% and 0.01% for the half-power bandwidth method from Table 3). Although the damping

Table 5. X and Y damping ratio obtained from the exponential decay method

Time Domain	X-axis	Y-axis
Target 1	No data	1.06%
Target 2	0.89% ±0.01%	0.96% ±0.02%

ratios at 0.89% and 0.96% are only 0.07% apart, it is a significant enough shift given the low standard deviation to show that the two axes of the target have different amounts of damping.

3.3 Target motion visualization

The *3D Visualization* component of the *Target Motion Characterization* GUI was used to interpret the target's motion path. One of the first applications of this GUI was to better understand cross-coupling. The time-domain transient excitation data, the same data used to calculate exponential decay damping, was run through the visualization GUI to see what the path of the target was and in particular to observe the target's motion along the unexcited axis. Three transient excitations were performed on the target with the same frequency and applied acceleration, with the only variable being the angle of the target about the Z-axis. Two-dimensional scatterplots of points the target occupied in the X-Y plane during the steady-state and damping periods were obtained, as shown in Fig. 7.

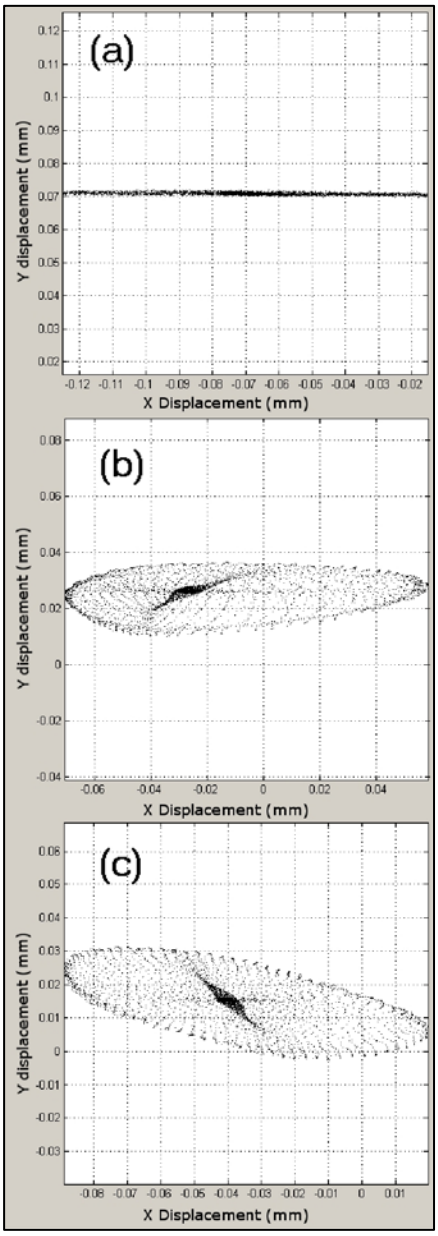

Fig. 7 X and Y target displacement with the target rotated at (a) 0º, (b) 20º, and (c) -45º
The target undergoes a complex motion path and displays cross-coupling when its principal axis is not aligned with the shaker's X-axis (b, c).

In Fig. 7(a), the target's X-axis is aligned with the shaker's X-axis, and so there is minimal cross-coupling along the shaker's Y-axis. In Fig. 7(b), however, the target has been rotated counterclockwise, evidently about 20º, as visible by the dense streak that indicates the target's X-axis, along which the target oscillates as it damps out. Under excitation,

the target oscillates clockwise along the roughly elliptical perimeter, and when the excitation is turned off, the motion path gradually changes to follow the straight, dense streak in the direction of the target's orientation. After a while, the target transitions to oscillating counter-clockwise along the small, dense elliptical shape near its stationary point. Further research is needed to fully understand the complex path of the target, which incorporates factors such as precession and different damping ratios and resonance frequencies for both target axes. These results show that the target acts most like a single degree of freedom system when its principal axes are aligned with the shaker's direction of acceleration, which is why tests were done in the 0º and 90º orientations only. Figure 7(c) reinforces the correlation. Here the target is rotated clockwise from the original position to approximately 45º, and the target's motion as it damps out is very similar to that of Fig. 7(b).

3.4 Target construction and motion behavior

Type 1 polyimide targets of the kind shown in Fig. 1 were compared with an experimental SiC target to establish general trends. Also, polyimide targets have several variables where they differ in construction, mainly because they are still manually and individually fabricated. The effect of these variables on target motion was also explored.

The experimental SiC target closely resembles the standard Type 1 targets in construction, except that the polyimide stalk section is replaced by a SiC stalk of similar diameter. Therefore, this stalk is much stiffer and less compliant than the polyimide stalks. As the SiC target construction is similar to that of the polyimide target, it is still asymmetrical, and so there are two primary resonance frequencies, as shown in Table 6. Note that the SiC target resonance frequencies are more than double the resonance frequencies obtained for the Type 1 polyimide targets, at around 364 Hz and 373 Hz for the X and Y axes, respectively.

Table 6. Properties of an experimental SiC target

SiC target	X-axis	Y-axis
Resonance frequency	364.1 Hz	372.8 Hz
Resonance transmissibility	183 µm/gn	216 µm/gn
Damping ratio	0.38%	0.35%

Transmissibility and damping values for the SiC target are averaged values from both the half-power bandwidth and exponential decay methods.

Table 6 also shows that the resonance transmissibility in the SiC target is virtually cut in half, from around 400 µm/gn to only around 200 µm/gn. This seems to support the trend that resonance modes at higher frequencies have lower transmissibility values. Furthermore, although the damping ratio is only around 0.4%, far lower than the 1% measured for Type 1 targets, this should not mean that the SiC target takes longer to reach a negligible amplitude than Type 1 targets. Preliminary tests indicate that due to the lower transmissibility causing a lower amplitude of oscillation, the total decay time to a negligible value for a SiC target is shorter than that of a Type 1 target, if both are given the same acceleration at resonance. Further testing of the total time needed for a target to reach negligible motion and the correlation with resonance frequency, transmissibility, and damping ratio is needed in order to confirm this hypothesis.

The three Type 1 targets tested showed variations in the diameter of the SiC stalk and the length of the polyimide stalk (see Table 7). These play a role in determining the overall stiffness of the target, which relates predictably to the target's resonance frequency, transmissibility, and damping ratio. In comparing the stiffer SiC target to the more compliant polyimide Type 1 target, it is seen that stiffer targets have a higher resonance frequency, lower transmissibility, and lower damping, given the same general target design but different materials. In Table 7, similar trends can be seen by comparing the properties of the type 1 targets.

Table 7 clearly shows a correlation between stiffness and resonance properties: Target 3, which has a thin SiC stalk and a long polyimide stalk, both making it more compliant, has the lowest resonance frequency of all three targets as well as the highest approximate

transmissibility. It is also the best damped, potentially due to the long polyimide stalk. Comparing targets 1 and 2 gives inconclusive results, because target 2 has a thicker SiC stalk than target 1, making it less compliant, but a longer polyimide stalk, making it more compliant.

Table 7. Target fabrication variables and resonance properties for Type 1 polyimide targets

	Target 1	Target 2	Target 3
SiC stalk diameter	17 μm	18 μm	16 μm
Polyimide stalk length	11.3 mm	11.7 mm	11.8 mm
Resonance frequency (X, Y)	148.8 Hz, 145.6 Hz	142.9 Hz, 150.9 Hz	134.1 Hz, 135.9 Hz
Resonance transmissibility	~400 μm/gn	~400 μm/gn	~450 μm/gn
Damping ratio (X, Y)	1.1%, 1.1%	0.9%, 1.0%	1.2%, 1.1%

Based on these results, further research will focus on creating target structures that maintain small transmissibility and high resonance frequency but are better damped. One experimental target structure that could have these properties has a polar mount configuration, where two strands of a ductile heavy metal fluoride glass called ZBLAN [9] connect to the capsule at its two poles, held together with a C-frame.

4 Conclusions

Measurements were made to characterize the damping behavior at resonance of cryogenic fusion targets used in the OMEGA laser. Frequency, transmissibility, and damping ratio data at resonance were collected and analyzed. It has been shown that Type 1 polyimide targets have relatively high damping at around 1% of critical as measured by two independent methods, and that a high damping value comes at the cost of relatively high transmissibility, which makes for larger amplitude oscillations. Comparisons between Type 1 targets and with experimental SiC targets suggest that the stiffness of the target influences the target's resonance and damping characteristics in predictable ways, at least for single-stalk target designs such as

these. Future research will test these findings on a larger number of Type 1 targets and also focus on developing new types of target mounts in order to increase the resonance frequency, decrease the transmissibility, and increase the damping.

A GUI program, *Target Motion Characterization,* has been written that analyzes experimental data and displays high frame rate visualizations of the target's path of motion under complex excitations in three dimensions. The visualization indicates that these targets have two principal axes at right angles to each other and that the shaker needs to excite the target along one of these axes in order to minimize the amount of cross-coupling present in the target's motion.

Ultimately, the goal is to be able to measure the frequencies and amplitudes of excitations from the target chamber, replicate them using the shaker setup, and then optimize the target design to produce the least transmissibility and thus the least motion. This will eventually lead to reduced target motion at the time of the laser shot, leading to more accurate positioning of the target in the OMEGA chamber center and thus increasing the uniformity of the implosion.

Acknowledgements

I would like to thank Mr. L. D. Lund for being my research advisor and helping me with the project; Dr. R. S. Craxton for reviewing my findings and suggesting improvements for this report; Mr. M. Bonino for providing guidance and test targets; and Dr. D. R. Harding for his advice and suggestions for experiments to perform.

References

[1] J. Nuckolls, L. Wood, A. Thiessen, and G. Zimmerman, "Laser compression of matter to super-high densities: thermonuclear (CTR) applications," *Nature*, vol. 239, pp. 139-142, Sept. 1972.

[2] T. R. Boehly et al., "Initial performance results of the OMEGA laser system," *Optics Communications,* vol. 133, pp. 495-506, January 1997.

[3] R. Orsagh et al., "Structural dynamics of cryogenic target assemblies," *LLE Review*, vol. 108, pp. 179-188, July-Sept. 2006.

[4] D. R. Harding et al., "Producing cryogenic deuterium targets for experiments on OMEGA," *Fusion Science and Technology*, vol. 48, pp. 1299-1306, Nov. 2005.

[5] T. C. Sangster et al., "Cryogenic DT and D_2 targets for inertial confinement fusion," *Physics of Plasmas*, vol. 14, pp. 1-10, April 2007.

[6] H. S. Cho, *Optomechatronics: fusion of optical and mechatronic engineering.* Boca Raton, Florida: CRC Press, Taylor & Francis Group, LLC., 2006, pp. 189-192.

[7] J. S. Bendat and A. G. Piersol, *Random Data: Analysis and Measurement Procedures, Third Edition*. New York: John Wiley & Sons, Inc., 2000, pp. 394-447.

[8] A. D. Nashif, D. I. G. Jones, and J. P. Henderson, *Vibration Damping*. New York: John Wiley & Sons, Inc., 1985, pp. 117-154.

[9] C. C. Chen, Y. J. Wu, and L. G. Hwa, "Temperature dependence of elastic properties of ZBLAN glasses," *Modern Chemistry and Physics*, vol. 65, pp. 306-309, Aug. 2000.